# Numerical Computation of the Fiber Diameter of Melt Blown Nonwovens Produced by the Inset Die

**Ting Chen, Chong Zhang, Xia Chen, Liqing Li**

*College of Textiles, Key Laboratory of Textile Science & Technology, Ministry of Education, Donghua University, Shanghai, 201620, People's Republic of China*

Received 9 August 2007; accepted 8 February 2008
DOI 10.1002/app.28611
Published online 31 October 2008 in Wiley InterScience (www.interscience.wiley.com).

**ABSTRACT:** Melt blowing is used commercially as a one-step process for converting polymer resin directly into a nonwoven mat of microfibers. The inset die is often used to produce polymeric fibers in the melt blowing process. The air jet flow field model for the dual slot inset die is established. The flow field model is solved by using the finite difference method. The numerical computation results of the air velocity distribution coincide with the experimental data. Then the air drawing model of polymers in the melt blowing process established in our previous research is solved with the aid of simulation results of the air jet flow field. The final fiber diameter of the nonwoven fabrics predicted by the air drawing model of polymers tallies with the experimental data. The results show the great potential of this research for the computer assisted design of melt blowing technology and equipment. © 2008 Wiley Periodicals, Inc. J Appl Polym Sci 111: 1775–1779, 2009

**Key words:** fibers; drawing; modeling; simulations

## INTRODUCTION

Melt blowing is used commercially as a one-step process for converting polymer resin directly into a nonwoven mat of ultrafine fibers. In the melt blowing process, high velocity hot air streams impact upon a stream of molten polymer as the polymer issues from a fine capillary. The result of this impact is that the polymer is rapidly (in about 50 μs) attenuated into fiber as fine as 1 μm in diameter. The fiber diameter of melt blown nonwovens, therefore, is strongly affected by the air jet flow field developed from the dual slot die as shown in Figure 1.

In our previous research, the air drawing model of polymers based on the numerical computation results of the air jet flow field in the melt blowing process was established.[1,2] The predicted distributions of the air velocity and air temperature and predicted fiber diameters of both polypropylene and polybutylene terephthalate (PBT) nonwovens showed good agreement with the experimental results.[1–3]

Our previous research has focused on the blunt die (without inset) as shown in Figure 1.[1,2] However, the inset die is often used to produce polymeric fibers in the melt blowing process. Figure 2 shows an inset die wherein the nosepiece tip is withdrawn a distance "*a*" into the body of the die. In this article, the air jet flow field model for the dual slot inset die will be established and solved numerically. And the fiber diameter of melt blown nonwovens produced by the inset die will be predicted with aid of the air drawing model of polymers.

## NUMERICAL COMPUTATION OF THE AIR JET FLOW FIELD

### The air jet flow field model

The air jet flow field model is established for the dual slot inset die used in the melt blowing process shown in Figure 2. The flow of two jets is assumed to be two-dimensional, steady and viscous. The most widely used turbulence model, the k-ε model, will be taken as the preferred turbulence model to yield accurate simulated results particularly in the case of high Reynolds numbers.

The air jet flow field model consists of five equations, i.e., the continuity equation, momentum

*Correspondence to:* T. Chen (chenting@mail.dhu.edu.cn).
Contract grant sponsor: National Natural Science Foundation of China; contract grant number: 50506007.
Contract grant sponsor: Foundation for the Author of National Excellent Doctoral Dissertation of China; contract grant number: 200761.
Contract grant sponsor: Shanghai Rising-Star Program; contract grant number: 05QMX1401.
Contract grant sponsor: Scientific Research Foundation for the Returned Overseas Chinese Scholars.
Contract grant sponsor: State Key Laboratory for Modification of Chemical Fibers and Polymer Materials, Donghua University, China.

Journal of Applied Polymer Science, Vol. 111, 1775–1779 (2009)

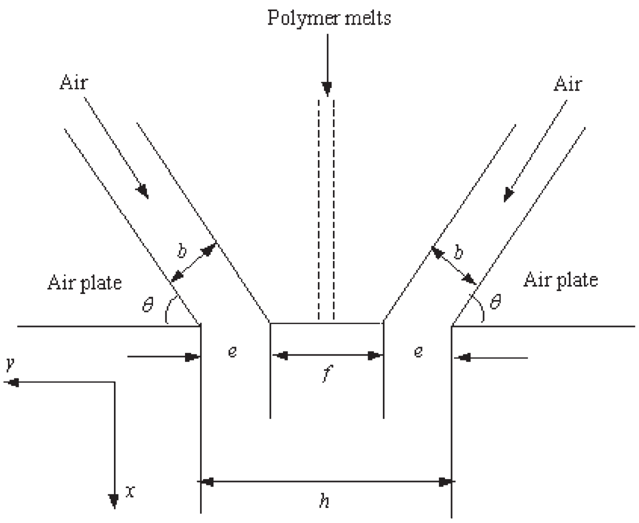


**Figure 1** Dual slot blunt die of melt blowing process.

equation, energy equation, turbulent kinetic energy equation, and turbulent dissipation rate equation.

Continuity equation:

$$\frac{\partial(\rho_a u_a)}{\partial x} + \frac{\partial(\rho_a v_a)}{\partial y} = 0 \tag{1}$$

where $\rho_a$ is the air density, $u_a$ is the $x$-component of air velocity, $v_a$ is the $y$-component of air velocity, $x$ is the axial position, and $y$ is the transversal position.

Momentum equation in $x$ direction:

$$u_a\frac{\partial(\rho_a u_a)}{\partial x} + v_a\frac{\partial(\rho_a u_a)}{\partial y} = \frac{\partial p_a}{\partial x} + 2\frac{\partial}{\partial x}\left[(\upsilon_a+\upsilon_t)\frac{\partial(\rho_a u_a)}{\partial x}\right] + \frac{\partial}{\partial y}\left\{(\upsilon_a+\upsilon_t)\left[\frac{\partial(\rho_a u_a)}{\partial y} + \frac{\partial(\rho_a v_a)}{\partial x}\right]\right\} + \frac{\theta_a - \theta_{am}}{\theta_{am}}g$$

$$\upsilon_t = C_\mu\frac{k_a^2}{\varepsilon_a} \tag{2}$$

where $p_a$ is the air pressure, $\upsilon_a$ is the kinetic viscosity of air, $\upsilon_t$ is the turbulent viscosity of air, $C_\mu$ is the constant of k-ε model, $\theta_a$ is the air temperature, $\theta_{am}$ is the ambient temperature, $g$ is the gravitational acceleration, $k_a$ is the turbulent dissipation rate of air, and $\varepsilon_a$ is the dissipation rate of turbulent kinetic energy of air.

Momentum equation in $y$ direction:

$$u_a\frac{\partial(\rho_a v_a)}{\partial x} + v_a\frac{\partial(\rho_a v_a)}{\partial y} = -\frac{\partial p_a}{\partial y} + \frac{\partial}{\partial x}\left\{(\upsilon_a+\upsilon_t)\left[\frac{\partial(\rho_a u_a)}{\partial y} + \frac{\partial(\rho_a v_a)}{\partial x}\right]\right\} + 2\frac{\partial}{\partial y}\left[(\upsilon_a+\upsilon_t)\frac{\partial(\rho_a v_a)}{\partial y}\right] \tag{3}$$

Energy equation:

$$u_a\frac{\partial(\rho_a\theta_a)}{\partial x} + v_a\frac{\partial(\rho_a\theta_a)}{\partial y} = \frac{\partial}{\partial x}\left[\frac{\upsilon_a+\upsilon_t}{\sigma_t}\frac{\partial(\rho_a\theta_a)}{\partial x}\right] + \frac{\partial}{\partial y}\left[\frac{\upsilon_a+\upsilon_t}{\sigma_t}\frac{\partial(\rho_a\theta_a)}{\partial y}\right] \tag{4}$$

where $\sigma_t$ is Prandtl number of turbulence.

Turbulent kinetic energy equation:

$$u_a\frac{\partial(\rho_a k_a)}{\partial x} + v_a\frac{\partial(\rho_a k_a)}{\partial y} = \frac{\partial}{\partial x}\left[\frac{\upsilon_a+\upsilon_t}{\sigma_k}\frac{\partial(\rho_a k_a)}{\partial x}\right] + \frac{\partial}{\partial y}\left[\frac{\upsilon_a+\upsilon_t}{\sigma_k}\frac{\partial(\rho_a k_a)}{\partial y}\right] - \frac{1}{\theta_{am}}\rho_a g\frac{\upsilon_t}{\sigma_t}\frac{\partial\theta_a}{\partial x} + (P_k - \varepsilon_a)\rho_a$$

$$P_k = (\upsilon_a+\upsilon_t)\left[2\left(\frac{\partial u_a}{\partial x}\right)^2 + 2\left(\frac{\partial v_a}{\partial y}\right)^2 + \left(\frac{\partial u_a}{\partial y} + \frac{\partial v_a}{\partial x}\right)^2\right] \tag{5}$$

where $\sigma_k$ is Prandtl number of turbulent kinetic energy.

Turbulent dissipation rate equation:

$$u_a\frac{\partial(\rho_a\varepsilon_a)}{\partial x} + v_a\frac{\partial(\rho_a\varepsilon_a)}{\partial y} = \frac{\partial}{\partial x}\left[\frac{\upsilon_a+\upsilon_t}{\sigma_\varepsilon}\frac{\partial(\rho_a\varepsilon_a)}{\partial x}\right] + \frac{\partial}{\partial y}\left[\frac{\upsilon_a+\upsilon_t}{\sigma_\varepsilon}\frac{\partial(\rho_a\varepsilon_a)}{\partial y}\right] + \rho_a(C_{\varepsilon 1}P_k - C_{\varepsilon 2}\varepsilon_a)\frac{\varepsilon_a}{k_a} - \frac{1}{\theta_{am}}gC_{\varepsilon 1}\frac{\varepsilon_a}{k_a}\frac{\upsilon_t}{\sigma_t}\frac{\partial(\rho_a\theta_a)}{\partial x} \tag{6}$$

where $\sigma_\varepsilon$ is Prandtl number of the turbulent dissipation rate, and $C_{\varepsilon 1}$, $C_{\varepsilon 2}$ are constants of k-ε model.

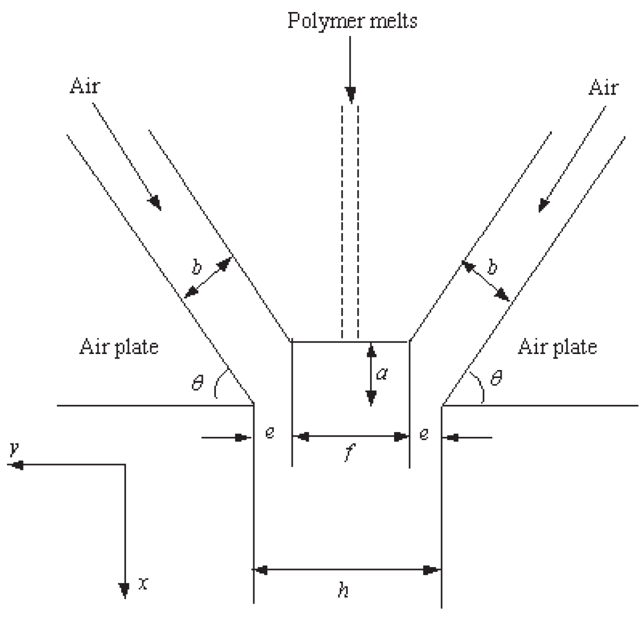


**Figure 2** Dual slot inset die of melt blowing process.

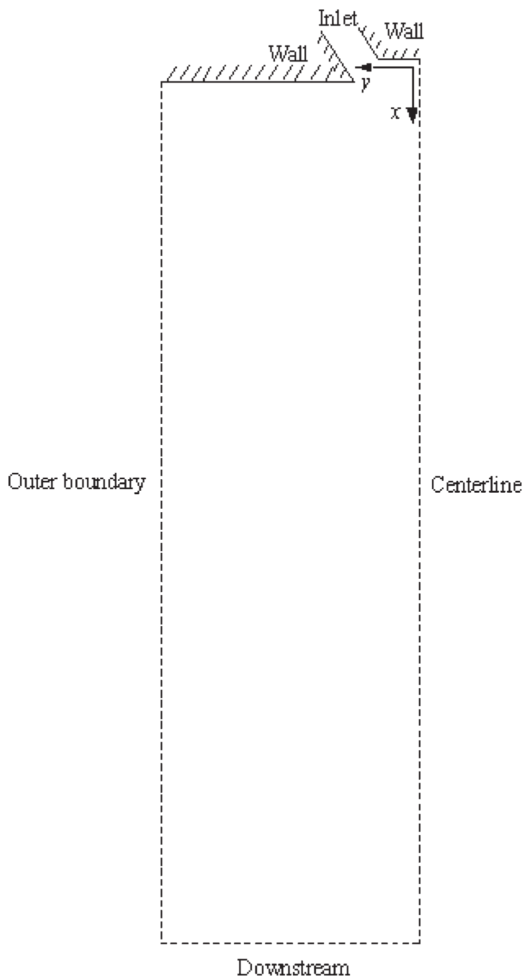


**Figure 3** Computational domain and boundary conditions.

First, the standard k-ε model is used for computation. Constants of the standard k-ε model are $C_\mu = 0.09$, $C_{\varepsilon 1} = 1.44$, $C_{\varepsilon 2} = 1.92$. Turbulent Prandtl numbers are as follows: $\sigma_t = 0.85$, $\sigma_k = 1.0$, $\sigma_\varepsilon = 1.3$, where $\sigma_t$, $\sigma_k$, and $\sigma_\varepsilon$ are Prandtl numbers of turbulence, of turbulent kinetic energy, and of turbulent dissipation rate. However, it is found that the standard k-ε model produces poor simulation results because of the great complexity of this air jet flow field. Therefore, the k-ε model of revised constants is adopted for computation. During the simulation procedure, it is found that the simulation results are very sensitive to $C_\mu$ and the turbulent viscosity $\upsilon_t$ is quite small for a region just below the die. According to Huai and Li[4] and our experiments, the width and height of this unique region are estimated to be $h$ and $(h + a)$, respectively. After trial calculations, it is found that simulation results coincide well with experimental results when $C_\mu = 0.025$ inside the near region and $C_\mu = 0.09$ outside this region. As a result, the k-ε model of revised constants stay utilized for our computation, where $C_\mu$ has different values in different regions while other constants stay the same values as those in the standard k-ε model.

Figure 3 shows the computational domain and boundary conditions. As the flow field is symmetrical along the system centerline, half of the plane is chosen as the computation area. The upstream boundary is on the nosepiece of the die. The downstream boundary is considered to be far enough from the die. The boundaries far enough from the system centerline are taken as the outer boundaries in $y$ direction. The boundary conditions are given below.

1. The conditions of upstream sections without inlet are:

$$u_a = 0 \quad v_a = 0 \quad \frac{\partial \theta_a}{\partial x} = 0 \quad k_a = 0 \quad \varepsilon_a = 0$$

   The conditions of upstream sections with inlet (in the slot) are:

$$u_a = u_{j0} \quad v_a = v_{j0} \quad \theta_a = \theta_{j0}$$

$$k_a = 0.06\left(u_{j0}^2 + v_{j0}^2\right) \quad \varepsilon_a = 0.06\frac{u_{j0}^3 + v_{j0}^3}{e}$$

   where $u_{j0}$ is the $x$-component of initial air velocity, $v_{j0}$ is the $y$-component of initial air velocity, and $\theta_{j0}$ is the initial air temperature.
2. Downstream section:

$$\frac{\partial u_a}{\partial x} = \frac{\partial \theta_a}{\partial x} = \frac{\partial k_a}{\partial x} = \frac{\partial \varepsilon_a}{\partial x} = 0 \quad v_a = 0$$

3. Centerline condition:

$$\frac{\partial u_a}{\partial y} = \frac{\partial \theta_a}{\partial y} = \frac{\partial k_a}{\partial y} = \frac{\partial \varepsilon_a}{\partial y} = 0 \quad v_a = 0$$

4. Outer boundary:

$$u_a = k_a = \varepsilon_a = 0 \quad \theta_a = \theta_{am} \quad \frac{\partial v_a}{\partial y} = 0$$

**Numerical methods for the air jet flow field model**

The air jet flow field model is solved by using the finite difference method. Below are some of the details. (a) The SIMPLE algorithm is used to solve the problem of velocity–pressure coupling. (b) The staggered grid is introduced to avoid the tooth-like distributions of velocity and pressure. (c) The power-law scheme is chosen as the preferred difference scheme. (d) The TDMA method is utilized to solve the difference equations.

In the computational domain, the coordinate origin is at the center of the die head. The $x$ direction is along the spinneret axis. The length ($x$-direction) and

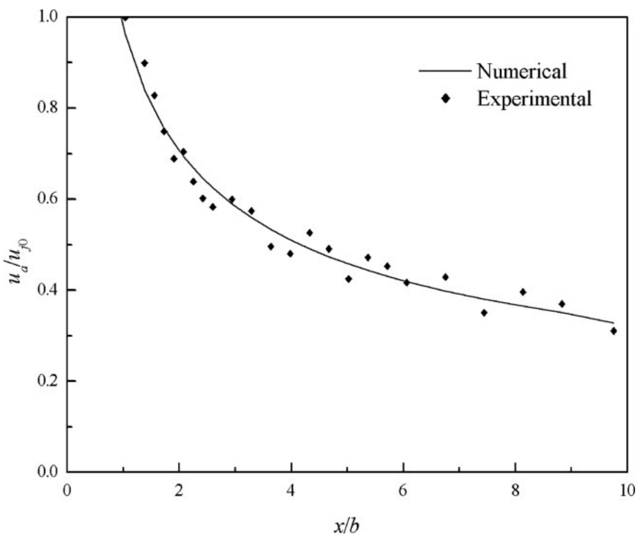


**Figure 4** Distribution of centerline $x$-component of air velocity along $x$-axis.

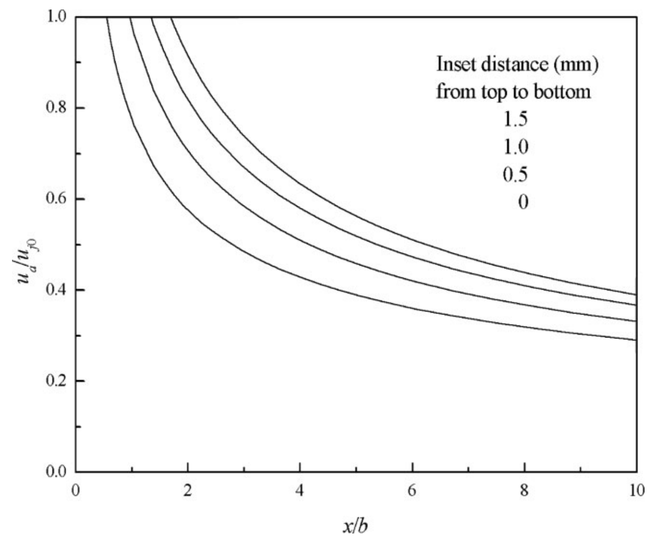


**Figure 5** Effect of the inset distance on air velocity distribution.

width ($y$-direction) of the computational domain are 200 mm and 60 mm, respectively. There are 400 grids in $x$ direction and 200 grids in $y$ direction.

### Comparison of numerical computation results with experimental data

To verify the flow field model, an analog die shown in Figure 2 is built to measure the air velocity distribution. Experiments are carried out on the flow field of the inset die shown in Figure 2. The head width, $f$, is 3 mm. The die length, $l$, is 50 mm. The air gap width, $b$, is 0.866 mm. The air slot angle, $\theta$, is 60°. The inset distance, $a$, is 0.5 mm. The air flow rate is 0.01 $m^3/s$. The initial air temperature is ambient temperature.

The air velocity is measured by IFA100 Hot Wire Anemometer produced by TSI Incorporated. To make full use of the output voltage range of the signal conditioner of IFA100, the offset and gain are calculated and set to be 1 v and 7.

The distributions of the centerline $x$-component of air velocity along $x$-axis are shown in Figure 4. The experimental data are represented by dots. It can be found that the numerical computation results obtained with the air jet flow field model fit well with the experimental data, which prove that the air jet flow field model can be used to predict the flow field of the inset die.

### Effect of the inset distance on air velocity distribution

To investigate the effect of the inset distance on the centerline $x$-component of air velocity, different inset distances of 0 (blunt die), 0.5, 1.0, and 1.5 mm are set in the numerical computations. Other die parameters such as the head width $f$, die length $l$, air gap width $b$, and air slot angle $\theta$ are kept unchanged. The air flow rate of 0.01 $m^3/s$ is maintained for all the computation runs.

Figure 5 shows the results of effects of the inset distance on the distribution of the $x$-component of air velocity along $x$-axis. It can be seen from the figure that the $x$-component of the air velocity decays rapidly along the $x$-axis after the air ejects from the slots. Larger inset distance will yield higher air velocity in the flow field, and the air velocity decay less rapidly along the $x$-axis. This is because increasing the inset distance $a$ will lead to a smaller slot width $e$. The same volume rate of air must pass through a smaller opening, so the air velocity increases.

## NUMERICAL COMPUTATION OF THE AIR DRAWING OF POLYMERS

The air drawing model of polymers in the melt blowing process established in one of our previous papers[1] is employed to predict the fiber diameter of melt blown nonwovens produced by the inset die. With the aid of numerical simulations of the air jet flow field, the distribution of the $x$-component of air velocity $u_a$ along the $x$-axis can be obtained. The air

**TABLE I**
**Measured and Predicted Fiber Diameter**

| | Sample A | Sample B |
|---|---|---|
| Measured fiber diameter (μm) | 7.794 | 2.766 |
| Predicted fiber diameter (μm) | 7.212 | 2.544 |
| Prediction error (%) | 7.46 | 8.02 |

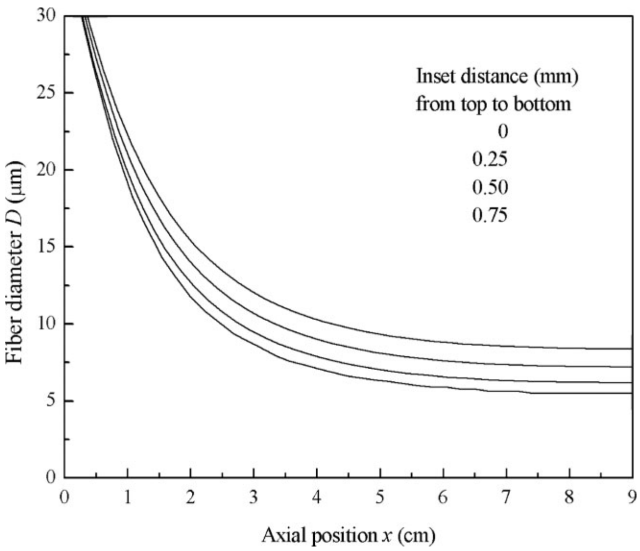


**Figure 6** Effect of the inset distance on fiber diameter.

drawing model of polymers is solved by using a fourth order Runge-Kutta method. Experiments are carried out on the melt blowing equipment at Shanghai Jiarong Filtering Material Corporation Limited. The spinneret hole diameter is 0.3 mm. The head width, $f$, is 0.5 mm. The die length, $l$, is 200 mm. The air gap width, $b$, is 0.22 mm. The air slot angle, $\theta$, is 60°. The inset distance, $a$, is 0.25 mm. Two polypropylene resins (A an B) with different melt flow rate are used in the experiment. The melt flow rate of Sample A is 37 g/10 min whereas that of Sample B is 1000 g/10 min. The polymer mass flow rate of Sample A and Sample B is 0.0786 g/s and 0.0634 g/s, respectively. Other processing parameters for Sample A and Sample B are the same. They have the initial air velocity of 194 m/s, the initial air temperature of 290°C, and the initial polymer temperature of 240°C.

The image analysis method is employed to measure the fiber diameter. The images of nonwoven samples are acquired with a Questar three-dimensional video frequency microscope (Questar Corp., New Hope, PA) with an enlargement factor of 600 and a depth of focus of 1 mm and then processed with Image-Pro Plus image analysis software (Media Cybernetics, Silver Spring, MD) to measure the fiber diameter. The image processing includes enhancement, smoothing, binarization, and filtering. The mean value of the diameters of 200 fibers is considered as the fiber diameter of a nonwoven sample. The measured fiber diameter, predicted fiber diameter, and prediction error of Sample A and Sample B are shown in Table I. It can be seen from the table that the prediction errors of both samples are quite small, which further confirm the effectiveness of our air drawing model of polymers.

Using the air drawing of polymers, the effect of the inset distance on the fiber diameter can be studied via computer simulations. All the die parameters and processing parameters for Sample A are kept unchanged as above except that the inset distance is 0, 0.25, 0.50, 0.75 mm in each simulation run, respectively. Figure 6 shows the effect of the inset distance on the fiber diameter. As expected, larger inset distances will produce finer fibers. When the inset distance is 0.75 mm, the final fiber diameter is 34.1% finer than that when the inset distance is 0 (blunt die). It is reasonable because a larger inset distance will yield a higher air velocity as just proved in the previous section. However, too large inset distance is not recommended in the melt blowing processing because fibers spun from an inset nosepiece may frequently stick to the air plates.

## CONCLUSIONS

The dual slot inset die is often used to produce polymeric fibers in the melt blowing process. The air jet flow field model for the dual slot inset die is established. The flow field model is solved by using the finite difference method. The numerical computation results of the air velocity distribution coincide with the experimental data. Computer simulations show that larger inset distance will yield higher air velocity in the flow field. The air drawing model of polymers in the melt blowing process is solved with the aid of simulation results of the air jet flow field. The final fiber diameter of the nonwoven fabrics predicted by the air drawing model of polymers tallies with the experimental data. It is found that larger inset distances can produce finer fibers. The results show the great potential of this research for the computer assisted design of melt blowing technology and equipment.

### References

1. Chen, T.; Huang, X. Model Simul Mater Sci Eng 2004, 12, 381.
2. Chen, T.; Wang, X.; Huang, X. Text Res J 2004, 74, 1018.
3. Chen, T.; Li, L.; Huang, X. J Appl Polym Sci 2005, 97, 1750.
4. Huai, W.; Li, W. J Hydrodyn Ser A 1994, 9, 112.